Differences in Fe-redox for asbestiform and nonasbestiform amphiboles from the former vermiculite mine, near Libby, Montana, U.S.A.†

MICKEY E. GUNTER,[1,2,*] M. DARBY DYAR,[3] ANTONIO LANZIROTTI,[4] JONATHAN M. TUCKER,[3] AND ELLY A. SPEICHER[3]

[1]Department of Geological Sciences, University of Idaho, Moscow, Idaho 83844, U.S.A.
[2]Marsh Professor-at-Large, University of Vermont, Burlington, Vermont 05405, U.S.A.
[3]Department of Astronomy, Mount Holyoke College, 50 College Street, South Hadley, Massachusetts 01075, U.S.A.
[4]Center for Advanced Radiation Sources, University of Chicago, 5640 S. Ellis Avenue, Chicago, Illinois 60637, U.S.A.

ABSTRACT

We obtained oriented Fe-XANES spectra on three amphibole bundles of fiber (i.e., asbestiform morphology), two single-crystal fragments (i.e., nonasbestiform morphology), and one aggregate of thousands of smaller particles (termed herein a "puffball") by use of a spindle stage mounted on beamline X26A, National Synchrotron Light Source, Brookhaven National Lab. These particles of differing morphology were obtained from a single rock sample collected at the former vermiculite mine near Libby, Montana, U.S.A. The XANES spectra vary as a function of orientation for the single-crystal fragments and bundles of fibers and were the same regardless of orientation for the puffball. Differences in the spectra for the single-crystal fragments and bundles of fibers indicate variations in Fe oxidation states between the two differing morphologies. Comparison to a calibration line based on amphibole standards allowed determination of $Fe^{3+}/\Sigma Fe$ values of 0.69 for the bundles of fibers and 0.60 for the single-crystal fragments, while the puffball had a $Fe^{3+}/\Sigma Fe$ value of 0.66. These values agree well with our earlier Mössbauer data on a bulk sample of this same material, with $Fe^{3+}/\Sigma Fe$ of 0.65. To our knowledge, these are the first data that show compositional differences between asbestiform and nonasbestiform amphiboles from the same sample. Because health effects appear to vary with amphibole morphology, these results suggest that iron oxidation, mineral morphology, and potential health effects may all be interrelated.

Keywords: Amphibole, asbestos, asbestiform, Fe-redox, XANES, spindle stage, Libby, Montana

INTRODUCTION

Over the past decade, heightened interest in the health effects of mineral dusts has been spurred by several events, including the exposure of amphibole asbestos to workers, their families, and residents of Libby, Montana (see Bandli and Gunter 2006; Gunter et al. 2007). Amphibole samples from that deposit have been compositionally characterized in a number of studies (Bandli et al. 2003; Gunter et al. 2003; Meeker et al. 2003; Sanchez et al. 2008).

In parallel to issues at Libby, debate continues about the differing health effects of asbestiform and nonasbestiform amphiboles. Most recent studies seem to indicate that the asbestiform habit is more harmful (Addison and McConnell 2008), which is significant because nonasbestiform amphiboles have not been regulated in the workplace by OSHA since as far back as 1992 (Gunter et al. 2007). Compositional differences may be related to morphology and health effects. Sanchez et al. (2008) showed that single-crystal fragments and fibers of Libby amphibole samples could be distinguished based on their trace element composition. Gianfagna et al. (2007) and Andreozzi et al. (2009) showed that asbestiform varieties have higher or comparable

$Fe^{3+}/\Sigma Fe$ relative to nonasbestiform fluoroedenites based on bulk Mössbauer analysis of samples from differing geological settings at the same location.

To date, it is still poorly understood why asbestos triggers disease. One hypothesis is that Fe might be a triggering agent (Van Oss et al. 1999), and two recent studies support this idea. Fantauzzi et al. (2010) used a suite of amphiboles of differing Fe oxidation states and found differences in cell mortality rates. Pacella et al. (2010) used the same suite of amphiboles and found variations in the production of oxygen free radicals as a function of Fe oxidation state.

The goal of this study was to build upon our earlier work in the development of a method to obtain $Fe^{3+}/\Sigma Fe$ from single-crystal fragments (Dyar et al. 2002a) along with previous Mössbauer (Gunter et al. 2003) and trace element (Sanchez et al. 2008) studies of Libby samples. We here use microfocused synchrotron X-ray absorption near-edge spectroscopy (micro-XANES) to characterize differences in the Fe oxidation state in amphiboles from a single rock as a function of morphology.

METHODS

A well-characterized richterite amphibole collected from the former vermiculite mine near Libby, Montana (Sanchez et al. 2008), was selected for this study. It is a unique hand sample because it contains intimately intergrown asbestiform and nonasbestiform amphibole particles with similar major element compositions (Sanchez et al. 2008; Gunter et al. 2007). We selected two perfect single-crystal fragments, three bundles of fibers, and one spherical agglomeration ("puffball")

---

of thousands of smaller particles for study (Fig. 1). Two kaersutites with different Fe-redox states from the USGS collections of Howard Wilshire and Robert Coleman (Dyar et al. 1993) were also studied to establish a calibration curve relating Fe X-ray absorption pre-edge peak energies and areas to Fe^{3+} contents: FR-12 is from a completely oxidized vent agglomerate in the Massif Central, France, Montgros ($Fe^{3+}/\Sigma Fe = 1.0$), while AK-M2 (Harrat al Kishb, Saudi Arabia) is dominantly Fe^{2+} ($Fe^{3+}/\Sigma Fe = 0.25$); see Dyar et al. (1993) for additional information.

XANES measurements were made at the synchrotron X-ray microprobe, beamline X26A at the National Synchrotron Light Source of Brookhaven National Laboratory, Upton, New York. A spindle stage was mounted with the plane of rotation perpendicular to the path of the focused X-ray beam (Dyar et al. 2002b). Single crystals were oriented optically by MEG using a polarizing light microscope equipped with a spindle stage. Each crystal fragment or bundle of fibers was mounted with the Z optical orientation nearly parallel to the rotation axis of a spindle stage; an additional orientation 90° from it was arbitrarily designated as Z'. For the crystal fragments, a polarizing light microscope was used to optically determine the X and Y optical orientations. In the fibers, X and Y were defined to be 90° from each other, with X as the thinner direction mimicking the shape of the single-crystal fragments (Fig. 1). This geometry allowed spectra to be acquired with the beam polarization direction directly parallel to the X, Y, Z, and Z' directions for the richterites, and X, Y, and Z for the kaersutites.

The incident X-ray beam was focused using two mutually orthogonal, 100 mm long, rhodium-coated silicon mirrors arranged in a Kirkpatrick-Baez geometry. The focused beam size on the sample was measured to be 7×9 μm (V × H). The incident X-ray beam was monochromatized using a Si(311) channel cut monochromator (Cottrell et al. 2009). The structure of the $FeK\alpha$ absorption edge was scanned in the near edge region. Incident beam energies were scanned from 7020–7105 eV at 0.5 eV increments, 7105.1–7118 eV in 0.1 eV increments, 7118.5–7140 in 0.5 eV increments, and 7141–7220 eV at 1.0 eV increments, using dwell times of 2, 15, 6, and 3 s, respectively. XANES spectra were collected in fluorescence mode using a 9-element, high-purity Ge, solid-state detector array. Spectra were edge-step normalized and corrected for self-absorption using the IFEFFIT Athena software package written by Ravel and Newville. The self-absorption correction utilized is the FLUO algorithm (D. Haskin, Univ. of Washington). Pre-edge peak energies were calibrated relative to the pre-edge centroid of a magnetite standard at 7113.25 eV.

In calculating the pre-edge energy and area, each spectrum was cropped to show only the pre-edge region. Centroid positions were extracted by simultaneously fitting the baseline with a linear function and a damped harmonic oscillator (DHO) function as described in Cottrell et al. (2009). The remaining pre-edge signal was fit using the Peak Analysis (PAN) processing package written by R.M. Dimeo of the NIST Center for Neutron Research. Each pre-edge was fit with two or three Lorentzian peaks, depending on the spectrum. Fits were repeated with slight variations in starting parameters until a consistent set of peak positions was obtained for the data set as a whole.

RESULTS AND DISCUSSION

Results of pre-edge fits, including centroid position (in eV), full-width at half maximum, peak height, area, and relative area, are given in Tables 1 and 2 and shown in Figures 2 and 3. A maximum of three peaks could be fit to any spectrum. The iron content in sample FR-12 is pure Fe^{3+}, and has only two peaks at 7114.28 ± 0.02 and 7112.88 ± 0.02 eV. The small standard deviations indicate that these peaks are remarkably consistent in position, although their intensities vary slightly with
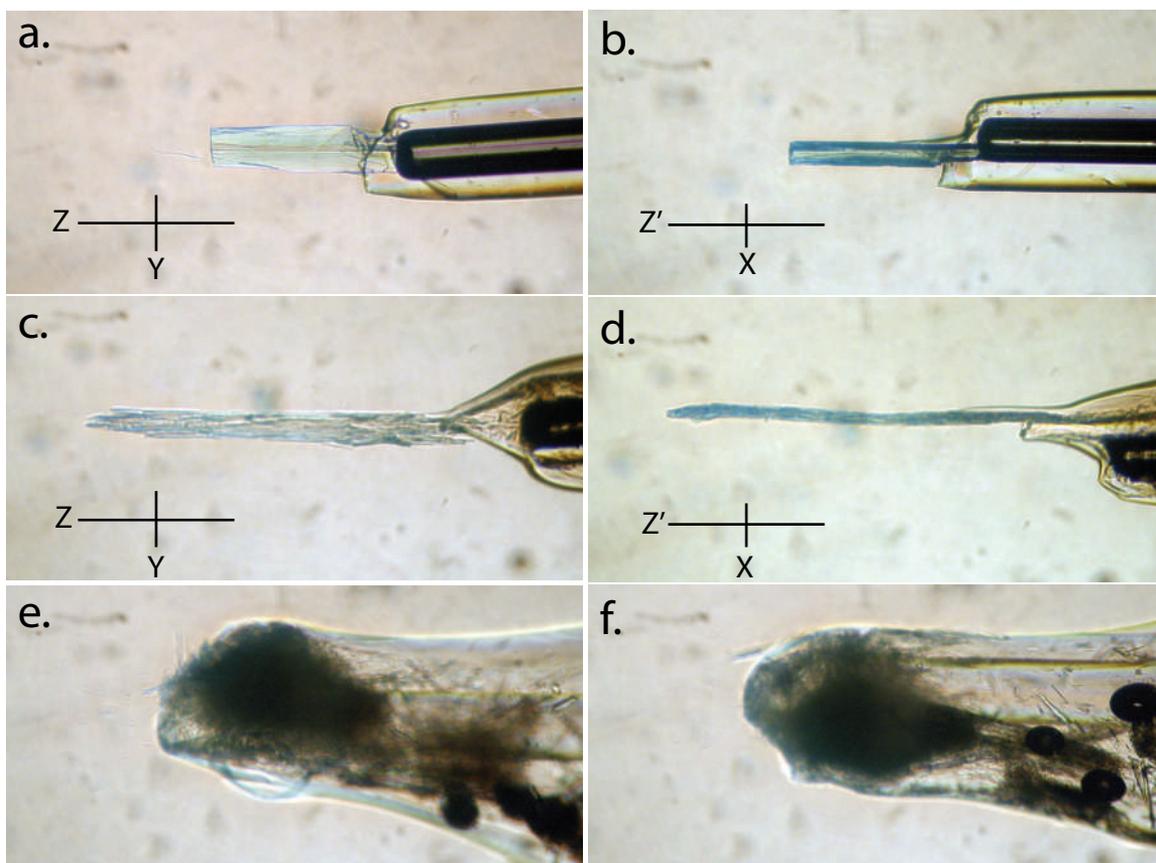
FIGURE 1. Photos of amphibole samples from the former vermiculite mine near Libby, Montana. (Top pair) A single-crystal fragment mounted with its c-axis parallel to the axis of spindle stage; in this orientation the sample can be rotated to collect XANES spectra with the polarized beam oriented parallel to Z and Y (in **a**) and Z' and X (in **b**). (Middle pair) A fibrous sample mounted with its c-axis parallel to the axis of spindle stage; in this orientation the sample can be rotated to collect XANES spectra with the polarized beam oriented along Z and Y (in **c**) and Z' and X (in **d**). In the lower pair of photos (**e** and **f**), a puffball (composed of thousands of randomly oriented particles) is shown; this sample would simulate a powder sample of the material, and its XANES spectra should be similar in all orientations. Field of view is approximately 300 μm.

TABLE 1. Summary of XANES results

Sample	Crystal fragment	Fiber bundle	Puffball	FR-12	AK-M2
Mössbauer %Fe^{3+}	65*	65*	65*	100†	25†
Fe^{3+} Centroid 1	7114.26 ± 0.07	7114.31 ± 0.06	7114.33 ± 0.01	7114.28 ± 0.02	7114.59 ± 0.13
Fe^{3+} ± Fe^{2+} Centroid 2	7113.22 ± 0.23	7113.11 ± 0.13	7113.02 ± 0.04	7112.88 ± 0.02	7112.93 ± 0.49
Fe^{2+} Centroid 3	7111.72 ± 0.30	7111.37 ± 0.03‡	7111.43 ± 0.09		7111.67 ± 0.45
Fe^{3+} Area 1	53 ± 9	44 ± 5	50 ± 5	78.95 ± 0.02	24.9 ± 0.1
Fe^{3+} + Fe^{2+} Area 2	33 ± 14	55 ± 7	30 ± 5	21.05 ± 0.02	47.2 ± 0.2
Fe^{2+} Area 3	18 ± 12	2 ± 4‡	10 ± 5		27.9 ± 0.3

Note: Fe^{3+} in richterite by Mössbauer is a bulk measurement of a ~30 mg mixture of fibers, fragments, and puffballs.
* Richterite data are from Sanchez et al. (2008).
† Kaersutite data are from Dyar et al. (1993).
‡ Two of the three single-crystal fragments have a third peak in the spectra with these parameters, but only when the beam is polarized parallel to the Z′ orientation.

TABLE 2. Orientation dependence of peak parameters

	Crystal fragment 1			Fiber bundle 3	
Parameter	Peak 1	Peak 2	Peak 3	Peak 1	Peak 2
X					
Area	0.1083	0.0269	0.0383	0.1065	0.0944
Relative area	62.4	15.5	22.1	53.0	47.0
FWHM	1.56	2.04	2.21	1.36	2.85
Height	0.0442	0.0084	0.0110	0.0499	0.0211
Centroid	7114.30	7113.42	7112.01	7114.20	7113.11
Y					
Area	0.0073	0.0041	0.0029	0.0548	0.0756
Relative area	51.2	28.8	20.0	42.0	58.0
FWHM	1.54	2.29	2.29	1.35	3.03
Height	0.0030	0.0011	0.0008	0.0258	0.0159
Centroid	7114.34	7113.29	7111.83	7114.25	7113.18
Z					
Area	0.0828	0.0273	0.0114	0.0529	0.0555
Relative area	68.1	22.5	9.4	48.8	51.2
FWHM	2.04	1.69	1.47	1.49	2.35
Height	0.0258	0.0103	0.0049	0.0226	0.0151
Centroid	7114.26	7112.84	7111.54	7114.27	7112.99
Z′					
Area	0.0376	0.0513	0.0135	0.0372	0.0601
Relative area	36.7	50.1	13.2	38.2	61.8
FWHM	1.59	1.72	1.60	1.38	1.96
Height	0.0151	0.0190	0.0054	0.0172	0.0196
Centroid	7114.41	7113.13	7111.44	7114.27	7112.97
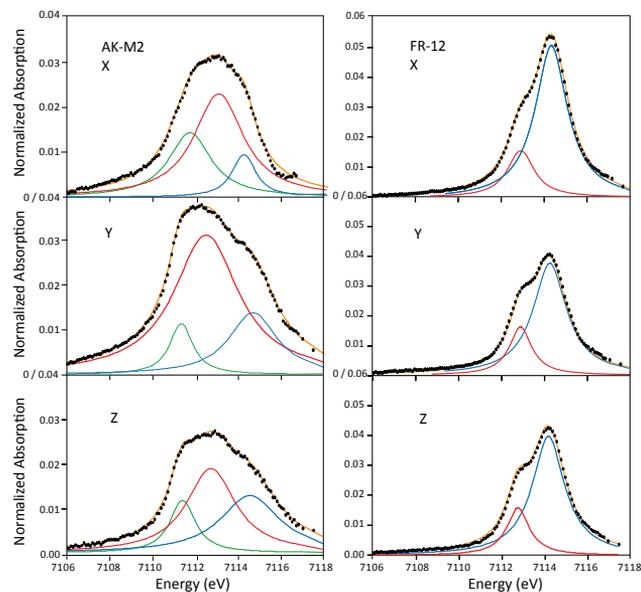
FIGURE 2. Kaersutite pre-edge fits. The blue peak has an energy of ~7114.3 eV and is assigned to Fe^{3+} only. The red peak at ~7113.1 eV probably represents some combination of overlapping Fe^{2+} and Fe^{3+} peaks, and the green peak at ~7111.4 eV is assigned to Fe^{2+} only (see Table 1). Sample AK-M2 has Fe^{3+}/ΣFe = 0.25, while FR-12 is Fe^{3+}/ΣFe = 1.0.

orientation. These peaks must result from Fe^{3+}. The spectra taken with the beam polarized along the *Y* and *Z* orientations are roughly similar in both shape and in intensity, while the spectra with the polarization parallel to the *X* orientation have a more intense peak at 7114.28 eV. In XANES spectroscopy, peak intensity predominantly reflects site asymmetry (a perfectly symmetrical site may have no pre-edge), while cation abundance has a lesser effect. So this increase in the peak intensity for spectra acquired with the beam polarization parallel to the *X* orientation probably reflects the more-distorted geometry of the Fe^{3+} sites in the *X* direction.

The iron content of AK-M2 is dominantly Fe^{2+} (Fe^{3+}/ΣFe = 0.25), so the two peaks observed in FR-12 are less prominent. Its spectrum consists of three peaks at 7114.59 ± 0.13, 7112.93 ± 0.49, and 7111.67 ± 0.45 eV with areas averaging 24.9 ± 0.1%, 47.2 ± 0.2%, and 27.9 ± 0.3%, respectively. The highest energy of these is probably caused by Fe^{3+}, because it lies close to the 7114.28 eV peak in FR-12, although the slight mismatch in centroid position may indicate either a small contribution from a Fe^{2+} peak or imprecision resulting from the smaller peak area. The middle, dominant peak is close to the 7112.88 eV Fe^{3+} peak in FR-12, and may represent Fe^{3+}. However, these two "Fe^{3+} peaks" represent 72.1% of the total peak area in a sample that has only 25% of the total Fe as Fe^{3+}. Either Fe^{3+} distorts the sites so their resultant peak intensity (and area; cf. Table 1) is inflated, or one or both of these peaks also has some contribution from Fe^{2+}. Assignment of the peak at 7111.67 eV can be unequivocally made to Fe^{2+}, because no peak with that energy is found in the completely oxidized FR-12. Note also that in AK-M2 spectra, the spectrum with the beam polarized parallel to *Y* has the greatest intensity (suggestive of greater distortion in that direction), while those with the beam polarized parallel to the *X* and *Z* orientations closely resemble each other.

In nearly all cases (three fibers, one puffball, and two of the fragments), the most intense spectra are those acquired with the beam polarized parallel to the *X* orientation (Fig. 3), again suggesting some pronounced asymmetry in that orientation. Each of these samples has spectra with centroids at roughly 7114.3, 7113.1, and 7111.4 eV, the same three energies observed in AK-M2 and FR-12. There are thus three fundamental peaks in these amphibole spectra that are not conspicuously dependent on bulk composition, because richterite (sodic-calcic amphibole subgroup) and kaersutite (calcic sub-group) are distinctive species.

The lowest-energy peak in the richterites is present across multiple orientations in the three fragments and in the puffball, although the puffball has only a small area in the low-energy peak, and its spectra could be modeled equally well without the third peak. These results suggest a consistent difference between fibers, puffball, and fragments. As seen in Figure 3 and Tables 1 and 2, the fragments consistently have three peaks in all four orientations relative to the polarized beam (*X*, *Y*, *Z*, and *Z′*). Only two of the fibers have the third, low-energy peak, and only in the *Z′* orientation, so the total area at ~7111.4 eV in the fibers' spectra is much lower than in those of the fragments. The spectra from
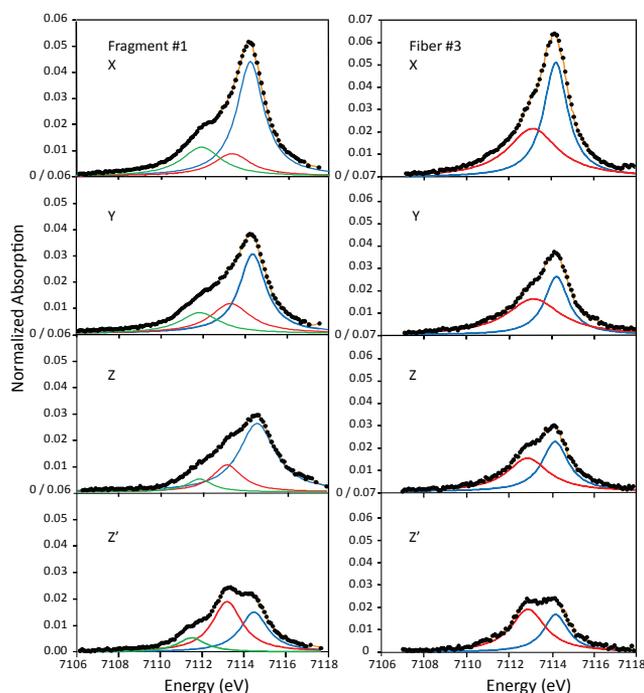
FIGURE 3. Pre-edge spectra of richterite single-crystal fragments and bundles of fibers, plotted on the same scale to showcase the relatively high intensity of the X orientation. The blue peak at 7114.3 eV is assigned to Fe^{3+}, the red peak at ~7113.1 eV may represent both Fe^{2+} and Fe^{3+}, and the green peak at ~7111.4 eV is likely Fe^{2+} (see Table 1). Note that the fiber bundle spectrum lacks a low-energy peak at ca. 7111.4 eV that is assigned to Fe^{2+}, so it is more oxidized than the fragment.

the fragments all have a consistent Fe^{2+} peak ca. 7111.4 eV, and are thus as a group more reduced than the fibers.

How much more reduced are the fibers and the puffball than the fragments? The 7111.4 eV peak has an average area of ~2% in the fibers, 10% in the puffball, and ~18% in the fragments. However, as noted earlier, this difference in peak area is not strictly proportional to the abundance of the species present, so predictions of $Fe^{3+}/\Sigma Fe$ content must be based on some combination of peak area and position. A simplistic calibration line can be made by calculating the average *a*rea-*w*eighted *centroid* ($centroid_{a-w}$) of each pre-edge (%$area_{peak1} \times$ position$_{peak1}$ + %$area_{peak2} \times$ position$_{peak2}$ + %$area_{peak3} \times$ position$_{peak3}$) and plotting this value vs. bulk Fe^{3+} concentration for the two "standards," AK-M2 and FR-12. The resultant straight line has a formula of $(Fe^{3+}/\Sigma Fe)_{pred} = 75.645 \times centroid_{a-w} - 538\,040$. This expression predicts that the $Fe^{3+}/\Sigma Fe$ concentration of the fibers is 0.69, the puffball 0.66, and the fragments 0.60. These results bracket the Mössbauer $Fe^{3+}/\Sigma Fe$ concentration of 0.65 for this sample (Sanchez et al. 2008).

Further work on a wider range of amphibole bulk compositions and $Fe^{3+}/\Sigma Fe$ is in progress to refine this calibration further (with only two end points, error analysis cannot be properly done). Regardless of the precise determination of the oxidation state of Fe in these samples, it is strongly suggested from the spectra in Figure 3 that the asbestiform Libby samples are more oxidized than the nonasbestiform. These differences may play a role in the causation of disease between these differing morphologies. To our knowledge, this is first time that a clear compositional distinction has been shown between asbestiform and nonasbestiform amphiboles from the same sample.

REFERENCES CITED

Addison, J. and McConnell, E.E. (2008) A review of carcinogenicity studies of asbestos and non-asbestos tremolite and other amphiboles. Journal of Regulatory Toxicology and Pharmacology, 52, S187–S199.

Andreozzi, G.B., Ballirano, P., Gianfagna, A., Mazziotti-Tagliani, S., and Pacella, A. (2009) Structural and spectroscopic characterization of a suite of fibrous amphiboles with high environmental and health relevance form Biancavilla (Sicily, Italy). American Mineralogist, 94, 1333–1340.

Bandli, B.R. and Gunter, M.E. (2006) A review of scientific literature examining the mining history, geology, mineralogy, and amphibole asbestos health effects of the Rainy Creek Igneous Complex, Libby, Montana USA. Inhalation Toxicology, 18, 949–962.

Bandli, B.R., Gunter, M.E., Twamley, B., Foit, F.F. Jr., and Cornelius, S.B. (2003) Optical, compositional, morphological, and X-ray data on eleven particles of amphibole from Libby, Montana, U.S.A. Canadian Mineralogist, 41, 1241–1253.

Cottrell, E., Kelley, K., Lanzirotti, A., and Fischer, R. (2009) High-precision determination of iron oxidation state in silicate glasses using XANES. Chemical Geology, 268, 167–179.

Dyar, M.D., Mackwell, S.M., McGuire, A.V., Cross, L.R., and Robertson, J.D. (1993) Crystal chemistry of Fe^{3+} and H^+ in mantle kaersutites: Implications for mantle metasomatism. American Mineralogist, 78, 968–979.

Dyar, M.D., Gunter, M.E., Delaney, J.S., Lanzarotti, A., and Sutton, S.R. (2002a) Systematics in the structure and XANES spectra of pyroxenes, amphiboles, and micas as derived from oriented single crystals. Canadian Mineralogist, 40, 1347–1365.

——— (2002b) Use of the spindle stage for orientation of single crystals for microXAS: Isotropy and anisotropy in Fe-XANES spectra. American Mineralogist, 87, 1500–1504.

Fantauzzi, M., Pacella, A., Atzei, D., Gianfagna, A., Andreozzi, G.B., and Rossi, A. (2010) Combined use of X-ray photoelectron and Mossbauer spectroscopies in the analytical characterization of iron oxidation state in amphibole asbestos. Analytical and Bioanalytical Chemistry, 396, 2889–2898.

Gianfagna, A., Andreozzi, G.B., Ballirano, P., Mazziotti-Tagliani, S., and Bruni, B.M. (2007) Structural and chemical contrasts between prismatic and fibrous fluoro-edenite from Biancavilla, Sicily, Italy. Canadian Mineralogist, 45, 249–262.

Gunter, M.E., Dyar, M.D., Twamley, B., Foit, F.F. Jr., and Cornelius, S.B. (2003) Composition, $Fe^{3+}/\Sigma Fe$, and crystal structure of non-asbestiform and asbestiform amphiboles from Libby, Montana, U.S.A. American Mineralogist, 88, 1970–1978.

Gunter, M.E., Belluso, E., and Mottana, A. (2007) Amphiboles: Environmental and health concerns. In Frank C. Hawthorne, Roberta Oberti, Giancarlo Della Ventura, Annibale Mottana, Eds., Amphiboles: Crystal Chemistry, Occurrences, and Health Concerns, 67, p. 453–516. Reviews in Mineralogy and Geochemistry, Mineralogical Society of America and the Geochemical Society, Chantilly, Virginia.

Meeker, G.P., Bern, A.M., Brownfield, I.K., Lowers, H.A., Sutley, S.J., Hoefen, T.M., and Vance, J.S. (2003) The composition and morphology of amphibole from the Rainy Creek Complex, near Libby, Montana. American Mineralogist, 88, 1955–1969.

Pacella, A., Andreozzi, G.B., and Fournier, J. (2010) Detailed crystal chemistry and iron topochemistry of asbestos occurring in its natural setting: A first step to understanding its chemical reactivity. Chemical Geology, 277, 197–206.

Sanchez, M.S., Gunter, M.E., and Dyar, M.D. (2008) Characterization of historical amphibole samples from the former vermiculite mine near Libby, Montana, USA. European Journal of Mineralogy, 20, 1043–1053.

Van Oss, C.J., Naim, J.O., Costanzo, P.M., Giese, R.F. Jr., Wu, W., and Sorling, A.F. (1999) Impact of different asbestos species and other mineral particles on pulmonary pathogenesis. Clays and Clay Minerals, 47, 697–707.